Hindawi
International Journal of Antennas and Propagation
Volume 2022, Article ID 5320561, 7 pages
https://doi.org/10.1155/2022/5320561

Research Article

Research and Design of Radiofrequency Antenna on LCD

Wanshan Zhu,[1,2] **Zhe Gao**,[1] **Zhuo Meng**,[2] **Chen Wang**,[3] **Yang Li**,[1] **Chunmei Wang**,[4] **and Yunwei Jia**[3]

[1]*Tianjin Sino-German University of Applied Sciences, Tianjin 300350, China*
[2]*Tianjin Bocopto Technologies Co Ltd., Tianjin 300393, China*
[3]*Tianjin University of Technology, Tianjin 300384, China*
[4]*Tianjin Light Industry Vocational Technical College, Tianjin 300350, China*

Correspondence should be addressed to Chunmei Wang; flyarea1886@163.com and Yunwei Jia; yunweijia@tjut.edu.cn

Received 14 February 2022; Revised 10 May 2022; Accepted 14 May 2022; Published 30 May 2022

Academic Editor: Miguel Ferrando Bataller

This work studies the electromagnetic field of a radiofrequency (RF) antenna on 7-inch liquid crystal display (LCD) and presents a new approach where the RF antenna is designed on LCD. This approach takes the magnetic field effect of LCD as an input parameter when building and simulating antenna models using the software Ansoft HFSS. After obtaining the PCB of the antenna, place the antenna on LCD, so that the antenna and LCD overlap up and down and measure the equivalent physical parameters as a whole. Last, use the vector network analyzer and Smith circle graph to tune the antenna system for completing the impedance matching of the whole system. This method breaks through the limitation that the card swiping area and the display area cannot be in the same area due to electromagnetic interference. It has changed the appearance design concept of the mobile point of sale (POS), and the antenna size can be 20%–100% of the POS display area. A contactless card read-write experiment for the proposed method has been carried out. Results showed the return loss is less than −30 dB, and the effective read-write distance of the antenna can reach about 5 cm. This design method provides a broader application prospect for mobile POS.

1. Introduction

Radiofrequency identification (RFID) technology is the key technology of contactless integrated circuit (IC) card payment, and it is a wireless identification technology. RFID technology originated in Britain and was used to identify the enemy and our aircraft in the Second World War. Antenna design is the most important part of the RFID system. Antenna raw materials, antenna shape, and antenna manufacturing process all determine the performance of the antenna [1–3]. Different antenna structures and antenna designs are determined by different application requirements [4–13]. The complete RFID system includes read-write terminal (RWT) and an electronic tag (ET). The RF signal coupling between them can be divided into electromagnetic backscatter coupling (EBC) and inductive coupling (INC). EBC is generally applicable to RFID systems with long distance and high-frequency band, and its identification distance is usually greater than 1 m. The operating frequency of INC is generally 125 kHz and 13.56 MHz, and the typical operating distance is not more than 10 cm [14–19]. In many cases, RWT has multiple antennas. Some decoupling techniques to reduce the coupling and electromagnetic interfaces between RWT and ET are important. Decoupling technology plays an important role in improving antenna isolation [20–27].

Financial POS, which is widely used in contactless payment, uses inductive coupling 13.56 MHz RFID technology. To prevent mutual interference between LCD and RF antenna, LCD and RF antenna of this traditional POS are generally arranged up-down or left-right layout. As shown in Figure 1(a), this is a traditional financial POS. The upper part of this POS is the LCD area and the lower part is the RF antenna area. Above is the display part and below is the card swiping part, so that the display area and the RF area do not overlap, that is, the two areas are not in the same area. This traditional design method limits the size of LCD used in POS, which increases the volume of POS [28–33].

(a) (b)

Figure 1: Two types of POS. (a) POS with up-down layout. (b) POS with antenna on LCD.

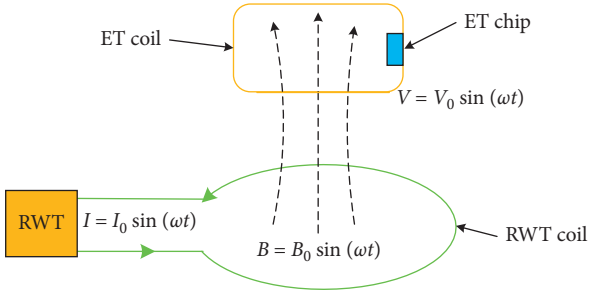

Figure 2: Schematic diagram of the RFID system. RWT, read-write terminal; ET, electronic tag.

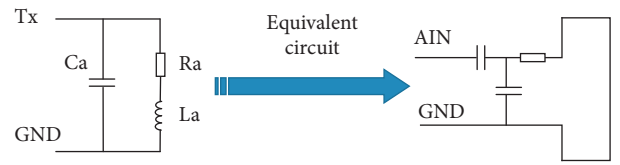

Figure 3: Equivalent circuit diagram of antenna coil. L_a, inductance; C_a, parasitic capacitance; R_a, parasitic resistance.

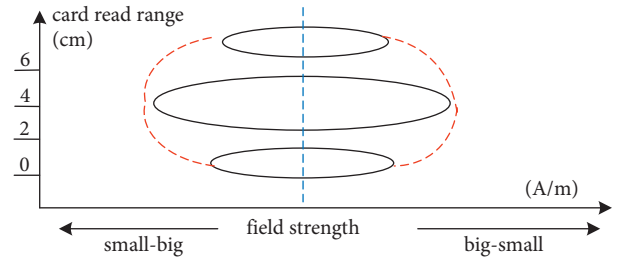

Figure 4: Field strength distribution within the card read-write distance.

2. System Composition

To solve that the card swiping area and the display area of POS cannot overlap because of electromagnetic interference, this study puts forward the design mode of overlapping up and down between LCD and RF antenna and expounds the design method of RF antenna. As shown in Figure 1(b), this is a POS designed using our proposed approach. The card swiping area of this POS is in the same area as the display area. The RF area and the display area overlap up and down, the front is the read-write antenna, and the back is LCD. The 13.56 MHz read-write antenna matching the LCD size is attached to LCD.

This design method and connection mode break through the limitation that the card swiping area and the display area cannot be in the same area due to electromagnetic interference, which effectively weakens the mutual interference between the RF antenna and LCD. It realizes that the display area is the card swiping area and changes the appearance design concept of POS. This design method expands the use area of POS, reduces the volume of POS, and widens the use scenario of POS.

3. Research on 13.56 MHz RF Antenna

As shown in Figure 2 [34], the inductive coupling mainly completes the transmission of signal and energy between coils through high-frequency alternating magnetic field. The inductive coupling 13.56 MHz RFID system is mainly composed of RWT and ET, in which ET is a passive tag. The RWT

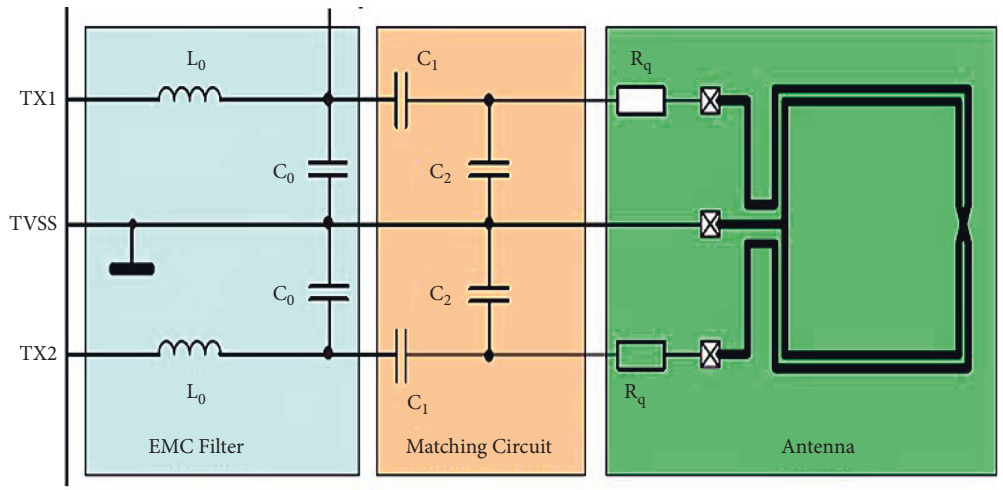

Figure 5: Antenna matching schematic diagram. *Rq*, damping resistance.

completes control, communication, and data storage, and ET also realizes the same function. When RWT needs to communicate with ET, the RWT coil converts the high-frequency current I into the spatial electromagnetic wave B, generating a high-frequency alternating magnetic field perpendicular to the coil plane; the ET coil entering the alternating magnetic field will have mutual inductance with the RWT coil, and ET obtains the voltage V through the induced current and the modulation information on the induced current. When RWT needs to receive, the RWT coil converts the electromagnetic wave intercepted from space into high-frequency current.

The common antenna coil forms are annular, square, and rectangular. The rectangular coil is chosen here. A rectangular antenna is a tuned LC circuit at a particular frequency. When the inductive impedance is equal to the capacitive impedance, the antenna will be at resonance. The equivalent circuit of the antenna coil is shown in Figure 3 [35], and the antenna coil is equivalent to a series resonant circuit composed of inductance L_a, parasitic capacitance C_a, and parasitic resistance R_a. The resonant frequency of the antenna can be obtained from Thomson formula (1).

$$f = \frac{1}{\left(2\pi\sqrt{L_a C_a}\right)}. \quad (1)$$

According to equation (1), the frequency of the antenna is only related to LC. When the resonant frequency f is constant, the larger the antenna size, the greater the inductance of the coil and the smaller the relative capacitance. In addition, to reduce the mutual interference between electronic components, the carrier field strength in the antenna induction area of the RWT should be within 1.5 A/m–7.5 A/m. The field strength distribution within the card swiping distance is shown in Figure 4.

4. Design of 13.56 MHz RF Antenna on LCD

This study uses the RF chip CLRC663 of the NXP Company and a 7-inch LCD to design the antenna system and obtains the reader antenna and matching circuit that meet the actual requirements. The CLRC663 works at 13.56 MHz. The antenna adopts a printed circuit board (PCB) rectangular antenna mode, and the antenna coil is attached to the 7-inch LCD. Figure 5 [35] shows a circuitry design with all relevant components required to connect an antenna to CLRC663. It ensures the transmission of energy and data between RWT and ET. The antenna matching schematic diagram is mainly composed of an electromagnetic compatibility (EMC) filter circuit, a network matching circuit, and an antenna coil circuit. The EMC is mainly used to filter out the third and fifth harmonics contained in 13.56 MHz and perform an impedance transformation. The network matching circuit acts as an impedance transformation block. The antenna coil circuit determines the quality factor of the antenna.

Figure 6 shows the circuit diagram of the POS RF part using the RF module CLRC663. It consists of three parts: the EMC filtering and network matching circuit at the transmitting end, the receiving circuit at the receiving end, and the transmitting and receiving antenna and its matching circuit.

In the design of the RF antenna on a 7-inch LCD, as shown in Figure 7, the antenna coil and impedance matching circuit are placed on the same PCB board. Considering the interaction between antenna parasitic capacitance and LCD parasitic capacitance, we add an open-circuit compensation coil at the end of the antenna coil to avoid the ground current and reduce the magnetic field strength of the antenna coil.

We use the electromagnetic simulation software Ansoft HFSS to establish the antenna model and determine the physical parameters of the antenna coil, including the length and width, line width, line spacing, thickness and number of turns, inductance value L, and resistance value R. The inductance value L is between 0.3 UH and 3 Uh, and the resistance value R is between 0.2 Ohm and 2 Ohm.

Figure 8 shows the antenna coil with a 7-inch LCD designed with Ansoft HFSS. The antenna coil is rectangular, with a length and width of 162 mm $*$ 97 mm. The composite substrate with high mechanical properties and high dielectric constant is selected as the antenna substrate. The

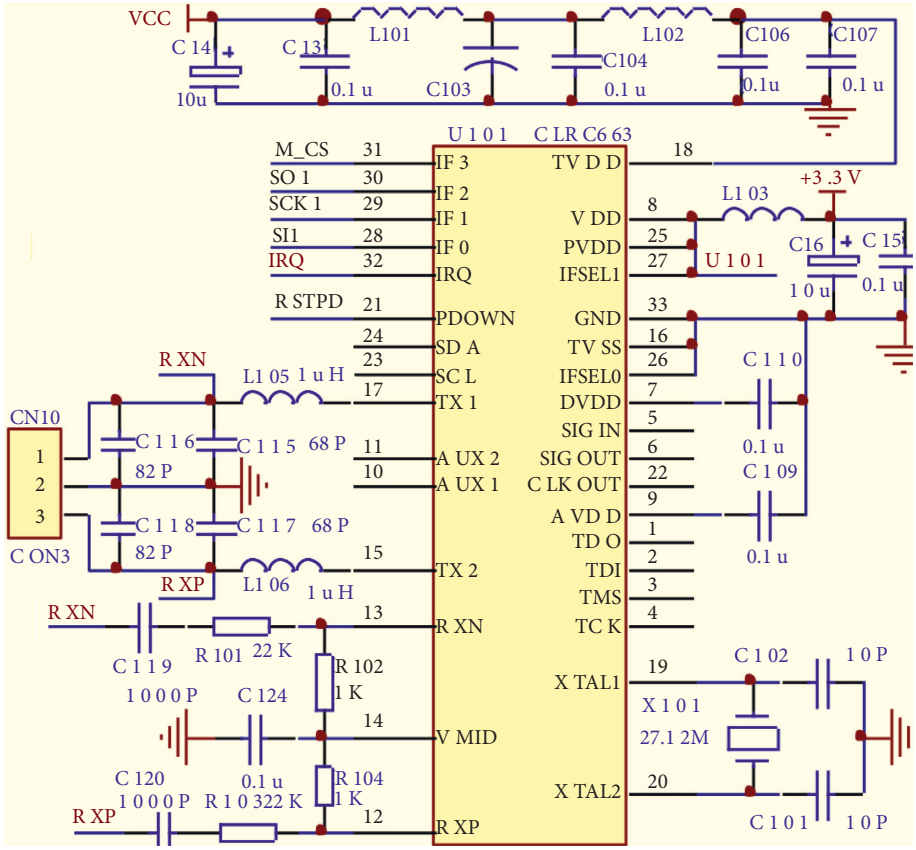

Figure 6: The circuit diagram of the POS RF part.

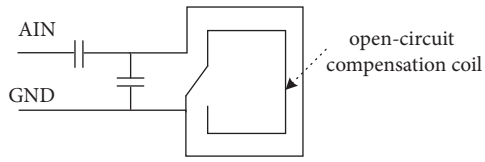

Figure 7: The antenna coil with an open-circuit compensation coil.

substrate is 1 mm thickness, the coil is 0.035 mm thickness and 3 mm width, and the material is copper foil with good conductivity to reduce the resistance loss of the coil.

After getting the designed PCB of the antenna coil, we can use the vector network analyzer or the calculation formula to obtain the equivalent circuit parameters of PCB, and according to the required value Q_q of the quality factor, calculate the damping resistance R_q. Here, we use the vector network analyzer to directly measure the inductance value L_a, parasitic capacitance C_a, and parasitic resistance R_a of PCB, as shown in Figure 3. The equivalent circuit must be determined under final environmental conditions, especially if the antenna will be operated in a metal environment or a ferrite will be used for shielding. Here, the 7-inch LCD must be placed under the antenna and measured by a vector network analyzer. If there is no vector network analyzer, equations (2) and (3) [35] can also be used to calculate L_a and R_a. C_a can be calculated by measuring the self-resonant frequency of the antenna or it can be approximated as a rule of thumb at 5 pF–10 pF.

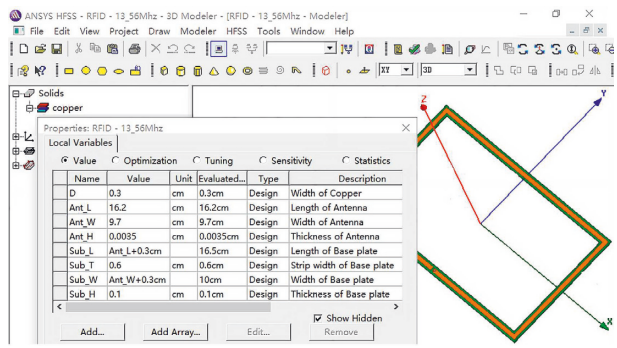

Figure 8: HFSS used to design the antenna coil on the 7-inch LCD.

Figure 9: An antenna that completed EMC filtering and impedance matching.

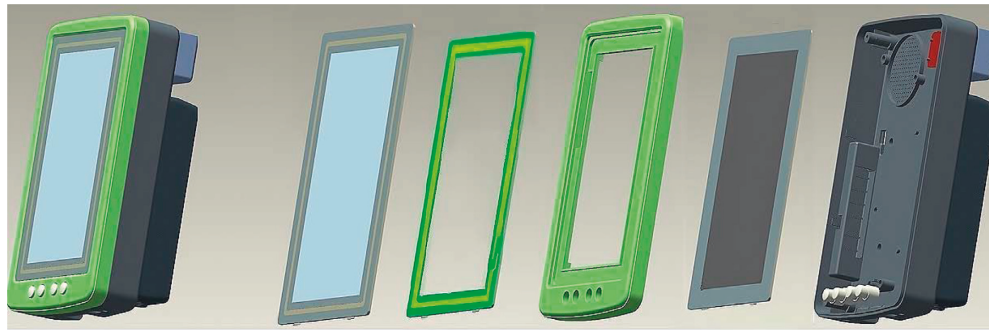

Figure 10: POS assembly diagram.

$$L_a \approx 2l\left(\ln\left(\frac{l}{D}\right) - \alpha\right)N^{1.8}, \tag{2}$$

where l is the single loop circumference of the coil, D is the line width, α is the rectangle factor of 1.54, and N is the number of turns of the coil.

$$R_a = \frac{\rho \mathrm{L}}{\mathrm{S}}, \tag{3}$$

where ρ is the resistivity of copper, L is the total length of the coil, and S is the cross-sectional area of the coil.

The quality factor Q_q represents the loss performance of the inductor coil. The higher the Q_q value is, the higher the antenna energy is. However, the higher the Q_q value is, the band-pass characteristics of RWT are affected. Generally, the Q_q value is between 10 and 30. Here, we take the quality factor $Q_q = 27$ (Mifare card) and then calculate the damping resistance R_q value according to (4) [35] and (5) [35].

$$Q_q = \omega\frac{L_a}{R_a}, \tag{4}$$

$$R_q = \frac{1}{2}\left[\frac{\omega L_a}{Q_q} - R_a\right]. \tag{5}$$

Antenna resonant frequency $f = 13.56\,\mathrm{MHz}$, so $\omega = 2\pi f = 8519999.27/\mathrm{s}$.

The specific parameters of the EMC filter circuit and network matching circuit are obtained by calculation. According to equations (6)–(11) [35], we can get C_0 of the EMC filtering circuit and C_1, C_2 of the network matching circuit, respectively, thus completing EMC filtering and impedance matching of the antenna system. Here, the cutoff frequency f_{ro} is 14.4 MHz, the matching resistance R_{match} is 20 Ohm between Tx1 and Tx2, and the inductance L_0 of the EMC filter circuit is 1000 nH.

$$C_0 = \frac{1}{(2\pi f_{ro})^2 L_0}, \tag{6}$$

$$X_{tr} = 2\omega\frac{L_0\left(1 - \omega^2 L_0 C_0\right) - \left(R_{\mathrm{match}}^2/4\right)C_0}{\left(1 - \omega^2 L_0 C_0\right)^2 + \left(\omega\left(R_{\mathrm{match}}/2\right)C_0\right)^2}, \tag{7}$$

$$R_{tr} = \frac{R_{\mathrm{match}}}{\left(1 - \omega^2 L_0 C_0\right)^2 + \left(\omega\left(R_{\mathrm{match}}/2\right)C_0\right)^2}, \tag{8}$$

$$R_{\rho a} = \frac{(\omega L_a)^2}{R_a + 2R_q}, \tag{9}$$

$$C_1 \approx \frac{1}{\omega\left[\sqrt{R_{tr}R_{pa}/4} + X_{tr}/2\right]}, \tag{10}$$

$$C_2 \approx \frac{1}{\omega^2 L_{pa}/2} - \frac{1}{\omega\sqrt{R_{tr}R_{pa}/4}} - 2C_{pa}. \tag{11}$$

Use the vector network analyzer to tune the antenna system. The C_0 of the EMC filter circuit, C_1, C_2 of the network matching circuit, and the damping resistance R_q are welded to actual PCB; then, the antenna coil is connected to the actual PCB. The vector network analyzer and the Smith circle diagram are used to tune the antenna system. Fix C_1, change the value of C_2 within a certain range, so that the imaginary part is zero to achieve the best effect, then fix C_2, debug the value of C_1, repeat this process until the best card reading effect is obtained, complete the overall antenna impedance matching, and obtain the maximum energy output. Figure 9 shows an antenna attached to a 7-inch LCD that has completed EMC filtering and impedance matching.

5. Experiment between RF Antenna and LCD

As shown in Figure 10, the designed antenna is placed above the upper shell, and then, LCD and the upper shell are tightly fixed, so that the position of LCD and the antenna coincide. From right to left, assemble the bottom shell, LCD, upper shell, antenna, and front panel and finally assemble the mobile POS, as shown in Figure 1(b).

The antenna design method is verified by experiments. In the experiment, we selected four tested PCB antennas, and their performance parameters are given in Table 1. The four antennas were assembled into four mobile POS, and then, the contactless card read-write test was carried out. The experimental results are given in Table 1. The optimal read-write distance is about 5 cm. As shown in Figure 11, in the working

Table 1: Antenna read-write distance.

POS	Antenna	Antenna L_a (uH)	Antenna R_a (Ω)	Card read distance S (cm)
1	1	0.86	0.14	4.9
2	2	1.03	0.13	5.0
3	3	0.87	0.13	5.1
4	4	1.04	0.14	4.9

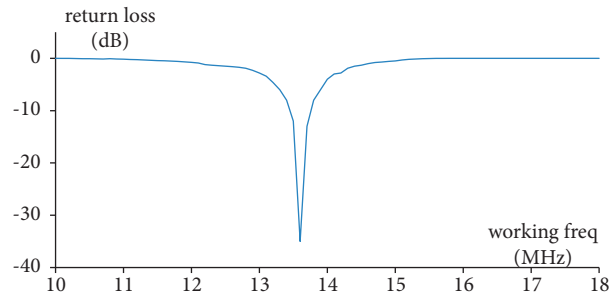

Figure 11: Antenna return loss after impedance matching.

frequency band, return loss is less than −30 dB and the reflection is very small, indicating that the antenna achieves good matching. The experiment proves that the antenna design is reliable and meets the performance requirements of the system.

6. Conclusion

This study presents a new approach where the RF antenna is designed on LCD. This method breaks through the limitation that the card swiping area and the display area cannot be in the same area. It has changed the design concept of POS, and the antenna size can be 20%–100% of the POS display area. The experiment results showed the return loss of the antenna is less than −30 dB, and the effective read-write distance of the antenna can reach about 5 cm. This approach expanded the scope of use of POS, reduced the volume of POS, and broadened the use scenario of POS.

Data Availability

Data sharing is not applicable to this article as no new data are created or analyzed in this study.

Conflicts of Interest

The authors declare that there are no conflicts of interest.

Acknowledgments

This study was supported by the Tianjin Natural Science Foundation (18JCYBJC19300) and 2019 Tianjin Jinnan District Science and Technology Commission Project (20190107).

References

[1] M. Alibakhshikenari and I. Huynen, "A comprehensive survey of metamaterial transmission-line based antennas: design, challenges, and applications," *IEEE Access*, vol. 8, Article ID 144778, 2020.

[2] I. Nadeem, M. Alibakhshikenari, F. Babaeian et al., "A comprehensive survey on 'circular polarized antennas' for existing and emerging wireless communication technologies," *Journal of Physics D: Applied Physics*, vol. 55, no. 3, p. 15, 2021.

[3] M. Alibakhshikenari, E. M. Ali, M. Soruri et al., "A comprehensive survey on antennas on-chip based on metamaterial, metasurface, and substrate integrated waveguide principles for millimeter-waves and terahertz integrated circuits and systems," *IEEE Access*, vol. 10, pp. 3668–3692, 2022.

[4] M. Alibakhshikenari, B. S. Virdee, C. H. See et al., "Dual-polarized highly folded bowtie antenna with slotted self-grounded structure for sub-6 GHz 5G applications," *IEEE Transactions on Antennas and Propagation*, vol. 70, 2021.

[5] M. Alibakhshikenari, S. Mansouri Moghaddam, A U. Zaman, J. Yang, B. Singh Virdee, and E. Limiti, "Wideband sub-6 GHz self-grounded bow-tie antenna with new feeding mechanism for 5G communication systems," in *Proceedings of the 13th European Conference on Antenna and Propagation (EuCAP) 2019*, Krakow, Poland, April 2019.

[6] M. A. Kenari, "Design and modeling of new UWB metamaterial planar cavity antennas with shrinking of the physical size for modern transceivers," *International Journal of Antennas and Propagation*, vol. 2013, Article ID 562538, 12 pages, 2013.

[7] M. Alibakhshikenari, A. Andújar, and J. Anguera, "New compact printed leaky-wave antenna with beam steering," *Microwave and Optical Technology Letters*, vol. 58, no. 1, pp. 215–217, 2016.

[8] M. Alibakhshikenari, B. S. Virdee, H S. Chan, R. A. Abd-Alhameed, F. Falcone, and E. Limiti, "Super-wide impedance bandwidth planar antenna for microwave and millimeter-wave applications," *Sensors*, vol. 19, no. 10, p. 2306, 2019.

[9] M. Alibakhshikenari, B S. Virdee, H S. Chan et al., "Study on improvement of the performance parameters of a novel 0.41–0.47 THz on-chip antenna based on metasurface concept realized on 50 μm GaAs-layer," *Scientific Reports*, vol. 10, no. 11034, pp. 1–9, 2020.

[10] M. Alibakhshi-Kenari, M. Naser-Moghadasi, R. Ali Sadeghzadeh, B. Singh Virdee, and E. Limiti, "New CRLH-based planar slotted antennas with helical inductors for wireless communication systems, RF-circuits and microwave devices at UHF–SHF bands," *Wireless Personal Communications*, vol. 92, no. 3, pp. 1029–1038, 2017.

[11] M. Alibakhshikenari, B. S. Virdee, A A. Ayman et al., "Study on on-chip antenna design based on metamaterial-inspired and substrate-integrated waveguide properties for millimetre-wave and THz integrated-circuit applications," *Journal of Infrared, Millimeter and Terahertz Waves*, vol. 42, no. 1, pp. 17–28, 2021.

[12] M. Alibakhshi-Kenari, M. Movahhedi, and H. Naderian, "A new miniature ultra wide band planar microstrip antenna based on the metamaterial transmission line," in *Proceedings of the 2012 IEEE Asia-Pacific Conference on Applied Electromagnetics (APACE)*, pp. 293–297, IEEE, Melaka, Malaysia, December 2021.

[13] M. Alibakhshikenari, B. S. Virdee, P. Shukla et al., "Metamaterial-inspired antenna array for application in microwave breast imaging systems for tumor detection," *IEEE Access*, vol. 8, Article ID 174667, 2020.

[14] L. H. Song and J. Z. Cui, "The design of passive RFID reader system based on MF RC500," *Advanced Materials Research*, vol. 1022, pp. 135–138, 2014.

[15] M. Guo, T. Chen, and C. Yu, "A novel embedded system for wireless ordering based on RFID," *Key Engineering Materials*, vol. 439-440, pp. 251–256, 2010.

[16] A. Chatterjee, S. Manna, R. Azizur, A R. Sarkar, A. Ghosh, and A. A. Alam, "An automated RFid based car parking system," in *Proceedings of the 2019 International Conference on Opto-Electronics and Applied Optics*, Kolkata, India, March 2019.

[17] S. A. Dewanto, M. Munir, B. Wulandari, and K. Alfian, "MFRC522 RFID technology implementation for conventional merchant with cashless payment system," *Journal of Physics: Conference Series*, vol. 1737, no. 1, 2021.

[18] Y. Norsuzila and M. Goon, M E. Mikail, H. Noor, M. Zikrul, A L. Yusof, and I. Azlina, RFID (NFC) application employment on inventory tracking to improve security," in *Proceedings of the IEEE Symposium on Wireless Technology and Applications, ISWTA*, pp. 176–181, IEEE, Kota Kinabalu, Malaysia, December 2014.

[19] S. Li, J. Lu, and S. Chen, "A room-level tag trajectory recognition system based on multi-antenna RFID reader," *Computer Communications*, vol. 149, pp. 350–355, 2020.

[20] A. Mohammad, B. Fatemeh, S. V. Bal et al., "A comprehensive survey on various decoupling mechanisms with focus on metamaterial and metasurface principles applicable to SAR and MIMO antenna systems," *IEEE Access*, vol. 8, Article ID 192965, 2020.

[21] A. Mohammad, S. V. Bal, and L. Ernesto, "Study on isolation and radiation behaviours of a 34 × 34 array-antennas based on SIW and metasurface properties for applications in terahertz band over 125–300 GHz," *Optik, International Journal for Light and Electron Optics*, vol. 206, Article ID 163222, 2020.

[22] M. Alibakhshikenari and B. S. Virdee, "Pancham shukla, chan hwang see. Isolation enhancement of densely packed array antennas with periodic MTM-photonic bandgap for SAR and MIMO systems," *IET Microwaves, Antennas & Propagation*, vol. 14, no. 3, pp. 183–188, 2020.

[23] M. Alibakhshikenari, B. S. Virdee, C. H. See et al., "Surface wave reduction in antenna arrays using metasurface inclusion for MIMO and SAR systems," *Radio Science*, vol. 54, pp. 1067–1075, 2019.

[24] M. Alibakhshikenari, M. Khalily, B. Singh Virdee et al., "Mutual-coupling isolation using embedded metamaterial EM bandgap decoupling slab for densely packed array antennas," *IEEE Access*, vol. 7, Article ID 5182, 2019.

[25] M. Alibakhshikenari, M. Khalily, B. Singh Virdee et al., "Mutual coupling suppression between two closely placed microstrip patches using EM-bandgap metamaterial fractal loading," *IEEE Access*, vol. 7, Article ID 23606, 2019.

[26] M. Alibakhshikenari, B. S. Virdee, P. Shukla et al., "Interaction between closely packed array antenna elements using metasurface for applications such as MIMO systems and synthetic aperture radars," *Radio Science*, vol. 53, no. 11, pp. 1368–1381, 2018.

[27] M. Alibakhshikenari, B. Virdee, P. Shukla et al., "Antenna mutual coupling suppression over wideband using embedded periphery slot for antenna arrays," *Electronics*, vol. 7, no. 9, p. 198, 2018.

[28] C. Xu, Y. Yan, and X. Liu, "Design of a long-range rectangular coil antenna for RFID access control system," in *Proceedings of the 2013 Loughborough Antennas and Propagation Conference*, pp. 420–423, IEEE, England, UK, November 2013.

[29] S. Wang, Y. Liu, and T. T. Ye, "Unconventionally shaped antenna design for UHF RFID tags," *International Journal of Antennas and Propagation*, vol. 20219 pages, Article ID 9965252, 2021.

[30] Y. Ma, H. Ning, W. Meng, and C. Tian, "Design and evaluation of a planar i-shaped folded-patch antenna for compact passive UHF RFID tags to cohere on metal," *Progress in Electromagnetics Research Letters*, vol. 94, pp. 49–55, 2020.

[31] T. Kunalen, L. Eng-Hock, B. Fwee-Leong, and C. Boon-Kuan, "Slim RFID tag antenna for metallic tools with narrow footprint," *IEEE Journal of Radio Frequency Identification*, vol. 5, pp. 182–190, 2021.

[32] F. You and Z. Jiang, "A broadband UHF RFID tag antenna design for metallic surface using module matching," *Progress in Electromagnetics Research Letters*, vol. 95, pp. 83–90, 2021.

[33] D. Cheng, Z. Wang, and Q. Zhou, "Analysis of distance of RFID system working under 13.56 MHz," in *Proceedings of the IEEE Wireless Communications, Networking and Mobile Computing*, pp. 1–3, IEEE, Dalian, China, October 2008.

[34] L. Youbok, "Antenna circuit design for RFID applications," *Microchip Technology Inc*, pp. 1–47, 2003.

[35] Antenna Design Guide, "Antenna design guide AN11019 CLRC663, MFRC630, MFRC631, SLRC610," 2012, https://www.radiolocman.com/shem/schematics.html?di=150570.